XLIII CILAMCE
21–25, November, 2022
FOZ DO IGUAÇU – PR – BRAZIL

Numerical modeling of the linking damage zone between geologic faults

Karoline N. Oliveira[1,2], Roberto Quevedo[2], Deane Roehl[1,2], Bruno R.B.M. Carvalho[3]

[1]*Civil and Environmental Engineering Department, PUC-Rio*
Rua Marquês de São Vicente, 225, 22453-900, Rio de Janeiro, Brazil
karoline@aluno.puc-rio.br, droehl@puc-rio.br
[2]*Tecgraf Institute, PUC-Rio*
Rua Marquês de São Vicente, 225, 22453-900, Rio de Janeiro, Brazil
karolinenunes@tecgraf.puc-rio.br, rquevedo@tecgraf.puc-rio.br, deane@tecgraf.puc-rio.br
[3]*Petrobras Research Center*
Av. Horácio Macedo, 950, 21941-915, Rio de Janeiro, Brazil
brcarvalho@petrobras.com.br

Abstract. Brittle fault zones are geological structures formed by a core and a damage zone that impact the fluid flow within geological formations. The fault core is usually responsible for the compartmentalization of several reservoirs acting as barriers while the damage zones may enhance the fluid flow. Both components present low seismic resolution that does not allow an appropriate characterization of those regions. Recent works based on the Finite Element Method (FEM) have focused on the characterization of damage zones adjacent to a geological fault. However, the interaction of two or more faults may create linking damage zones and preferential flow paths or barriers to fluid flow. This paper presents a methodology for the numerical modeling of damage zones resulting from the interaction between two geologic faults. Several scenarios of different relative distances between two faults are analyzed to understand the effect of linking damage zones.

Keywords: numerical modeling; fault damage zones; linking damage zone.

1 Introduction

Fault zones are complex geological structures formed by different deformation mechanisms in rocks. Those structures include a core and a damage zone, which concentrate different deformation levels and can impact the fluid flow of several reservoirs. Thus, their study and characterization are of great interest for developing production strategies and exploration in the oil and gas industries[1]–[5]. The fault core corresponds to the region with the highest levels of compressive deformation formed by fault rocks, as breccias and cataclasites that can act as fault seal. The damage zone is the region adjacent to the fault core constituted by a network of subsidiary structures. The identification of the damage zone in geological formations presents many uncertainties due to the low seismic resolution that does not allow a good characterization. However, some studies [2], [3] indicate that in highly porous rocks, the deformation mechanisms can cause grain reorganization and breakage, resulting in different types of deformation bands. On the other hand, rocks with low porosity normally respond to the same stress by fracturing. These geological structures can have considerable impacts on rock permeability. In other words, the damage zone can act as a conduit if fractures are dominant, while in the predominance of deformation bands the damage zones act as barriers [3], [6]. Kim et al.[7] defines three types of damage zone within and around a fault zone, as illustrated in Fig. 1.

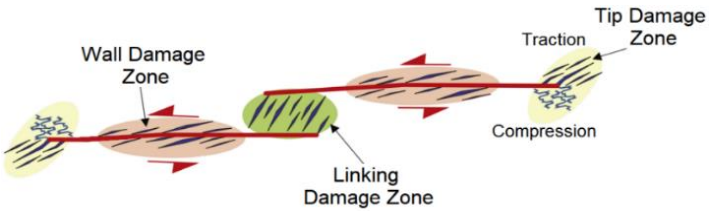

Figure 1. Types of interaction damage zone (Adapted from Peacock et al.[8]).

The tip damage zone is the rock volume deformation area that develops in response to a stress concentration around a fault tip. It may present contractional or extensional regions, depending on the fault formation mechanism. Wall damage zones are the regions resulting from the propagation of faults through rock or from damage associated with the increase in fault slip. The interaction of two or more faults generates the linking damage zone that can present different structures depending on the interaction between the two fault segments [7], [8].

Recent studies have characterized the damage zone corresponding to one fault [9], [10]. However, several uncertainties still exist, particularly regarding the definition of the geological structures that compose the linking damage zone between two or more faults. To understand the formation and development of linking damage zones, this study presents a methodology for numerical modeling of the interaction between two normal faults within carbonate reservoirs. Some scenarios considering different relative distances between two faults are analyzed.

2 Methodology

In this study, we assume that a normal fault can be represented through a vertical section under plane strain conditions, as shown in Fig. 2a. The fault is given by two superimposed straight lines inserted within a homogeneous porous medium. Over each line of the fault, displacements in opposite directions are applied incrementally to generate the damage zone. Those displacements are imposed considering a constant fault length and a parabolic distribution [11], Fig. 2b, with null displacements at the fault tips and maximum displacement (d_{max}) at the fault center. The value of d_{max} is defined as 10% of the total fault length (L) [12]. We restrict horizontal and vertical displacements in the nodes at model boundaries. Such boundaries are located far from the faults to avoid influencing the results. The finite element mesh is composed of elements of quadratic interpolation and full integration (CPE6, CPE8), as it is shown in Figure 2c.

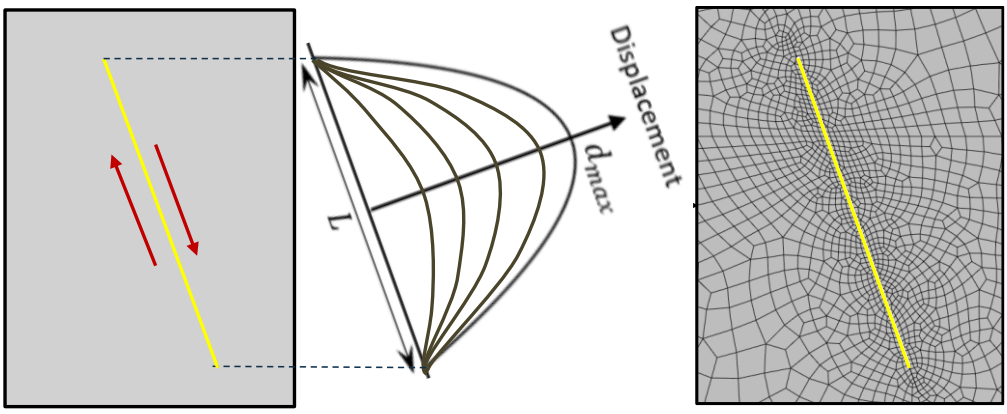

(a) (b) (c)

Figure 2. Model geometry (a), displacements imposed over the two faces of the fault (b) and the finite element mesh (c).

The Mohr-Coulomb elastoplastic model with a non-associated flow rule is used to represent the geomechanical behavior of the porous rock. The plastic regions triggered in the rock due to the application of

displacements along the nodes in the fault are considered the damage zone. To visualize those regions, we use the scalar variable PEMAG that is obtained through the principal plastic strains as follows:

$$PEMAG = \sqrt{\frac{2}{3}({PE_{P1}}^2 + {PE_{P2}}^2 + {PE_{P3}}^2)}. \quad (1)$$

Furthermore, in order to analyze better the behavior of the linking damage zone, we use p-q diagrams. The variable p is the average stress while q is the deviatoric stress; both stress invariants are given as:

$$p = \frac{\sigma'_1+\sigma'_2+\sigma'_3}{3}, \quad (2)$$

$$q = \sqrt{\frac{1}{2}[(\sigma'_1 - \sigma'_2)^2 + (\sigma'_1 - \sigma'_3)^2 + (\sigma'_2 - \sigma'_3)^2]}, \quad (3)$$

where σ'_i represents the principal effective stresses.

The simulations are performed with the software Abaqus® using the solver for large displacements and updated Lagrangian formulation.

3 Numerical Tests

The tests performed in this study consider two normal faults with the same length (L=500 m) and dip (θ=60°) as shown in Fig. 3. Two groups of models were built, the first varying the distance between the faults (A) and the second varying their overlapping (B). In all tests, we consider that the average depth between the shallowest and the deepest tips is 5000 m. The rock material parameters are listed in Tab. 1 and are typical of carbonates present in pre-salt reservoirs[13].

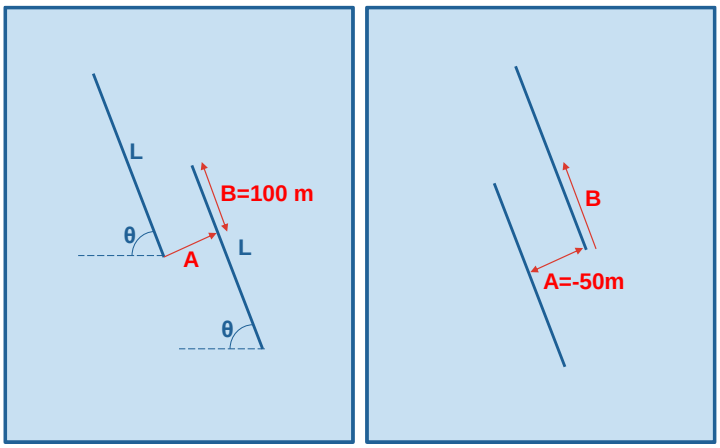

Figure 3. Geometrical settings of the parametric study.

Table 1. Carbonate rock parameters taken from [13].

Parameter	Carbonate	Unit
Young modulus (E)	17000	MPa
Poisson ratio (v)	0.3	-
Friction angle (Ø)	34.0	(°)
Dilatancy angle (ψ)	24.0	(°)
Cohesion (c)	6.0	MPa

The effective vertical stresses are assessed with a vertical stress gradient of 12 MPa. The horizontal stresses are obtained from the vertical ones considering a horizontal stress ratio of 0.9.

The first models were built considering a fixed B value of 100 m and A values equal to -200 m, -50 m, 50 m, e 200 m. Figure 4 shows the PEMAG contour plots at the end of each simulation. For the case A = -200 m, the

development of a linking damage zone between the faults is unclear. However, for the other A values, the linking damage zone is noticed with different PEMAG distributions in each case. The red arrows, which show the movement of the rock on both sides of the normal faults, can explain those differences. Negative or positive values of A lead to extension or compression of the region between the faults, respectively.

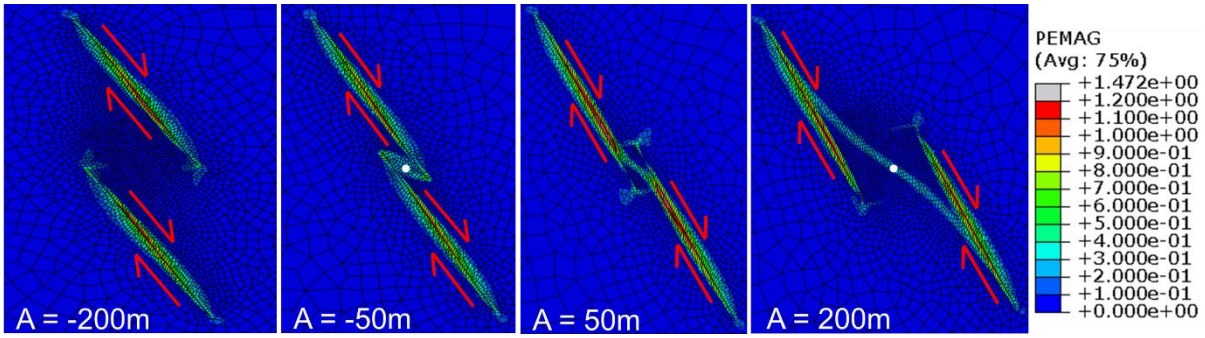

Figure 4. Results for models with different values of the distance between faults A.

In order to analyze the results better, we draw the stress paths of the two Gauss points (GP) indicated by white circles within the linking damage zone of the models with A=-50m and A=200m. Figure 5 shows the stress path of the GP for A = -50 m. We notice that the GP is under an elastic regime in the initial condition. However, after applying the prescribed displacements along the fault, the stress path goes to the left of the p-q diagram, surpasses the Mohr-Coulomb envelope, and reaches negative values of the stress invariant p (named "Pressure" in Abaqus). Those results indicate that this region is prone to developing fractures.

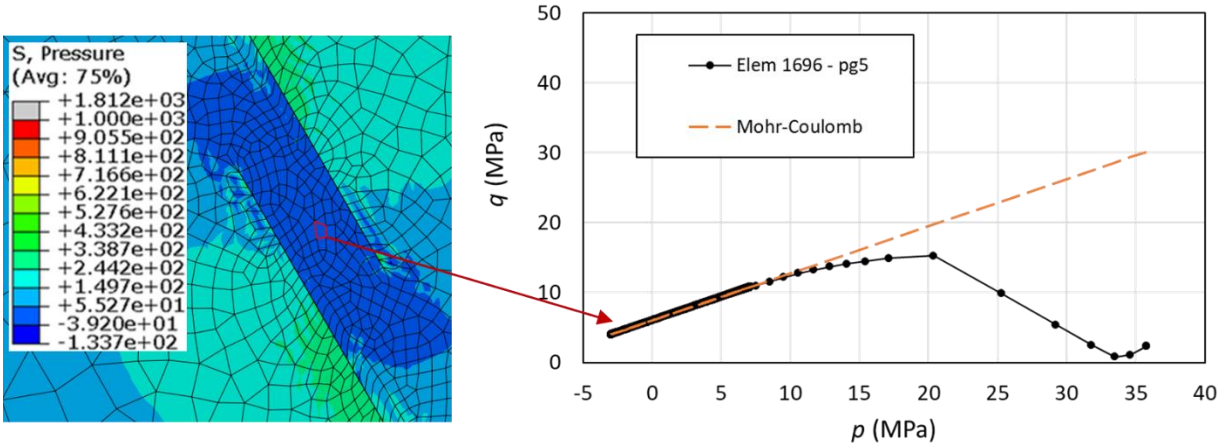

Figure 5. Stress path of a Gauss point within the linking damage zone of the model with A=-50m.

Figure 6 shows the GP stress path with A = 200 m. As in the previous case, the initial stress is under an elastic regime and reaches the Mohr envelope. However, in this case, the stress path goes to the right of the p-q diagram, increasing the stress invariant p to high values around 480 MPa. Those results indicate that the linking damage zone in this model is prone to develop compaction structures.

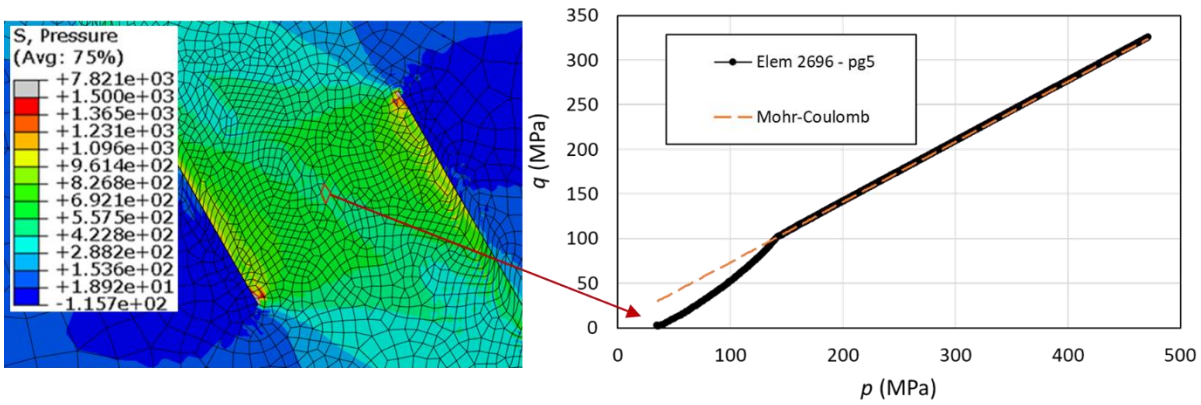

Figure 6. Stress paths of a Gauss point within the linking damage zone of the model with A=200m.

In the second group of tests, we varied the overlapping between the faults considering values of -200 m, -100 m, 100 m and 200 m, maintaining the distance A at -50m. The results in terms of PEMAG at the end of each simulation are shown in Figure 7. Once again, we notice that depending on positive or negative values of B, the linking damage zone presents different shapes; for negative values, extensional regions with narrow linking damage zones are triggered. On the other hand, for positive values, compressional regions with broad linking damage zones are produced.

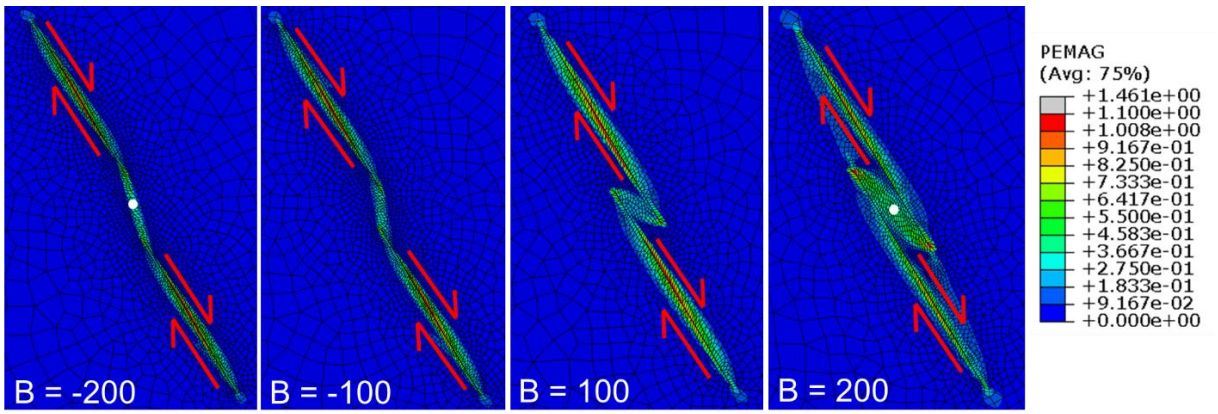

Figure 7. Results for models with different values of the overlapping B.

We draw the stress paths of the two Gauss points (GP) indicated by white circles within the linking damage zone of the models with B=-200 m and B=200 m. Figure 8 shows the stress path followed by the GP in the model with B = -200 m. The stress path reaches the Mohr-envelope and over this goes to the left of the diagram p-q, reducing the stress invariant p. Those values indicate that shear or dilation structures can be present in the linking damage zone.

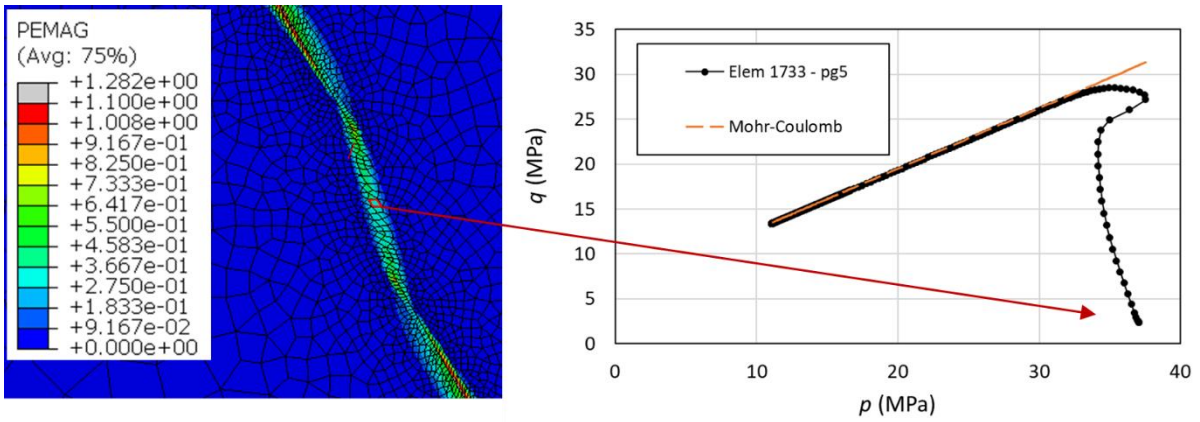

Figure 8. A Gauss point's stress path within the model's linking damage zone with B=-200 m.

Figure 9 shows the stress path of a GP located within the linking damage zone of the model with B=200 m. In this case, the stress path reaches the Mohr-envelope and follows it to the right of the diagram p-q. The stress invariant p increases reaching values of 900 MPa. Those values indicate that shear and compaction structures can be present in the linking damage zone.

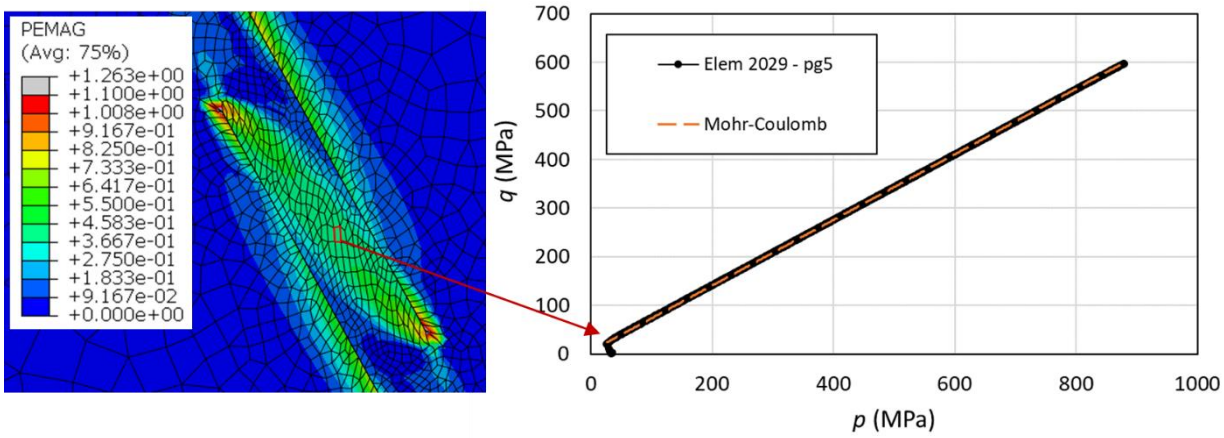

Figure 9. A Gauss point's stress path within the model's linking damage zone with B=200 m.

4 Conclusions

In this study, we focus on the interaction of two normal faults and analyze the linking damage zone triggered in carbonate rocks. Considering the FEM and the elastoplastic Mohr-Coulomb model with non-associated flow rule, we simulate the formation and evolution of damage zones through the imposition of displacements to the nodes located over two parallel faults. From the two groups of models analyzed, we observed that the linking damage zone presents extensional or compressional regions, depending on the relative position of the geological faults. Moreover, the stress paths of some representative points within the linking damage zone show that these regions are prone to fracturing, to develop deformation bands or other kinds of geological features. These results can be used to characterize linking damage zones in some rocks, allowing the identification of barriers or preferential flow paths. Further simulations also considering faults with different dips and lengths are under analysis to understand better the geomechanical behavior of linking damage zones.

Acknowledgments. This research was carried out in association with the ongoing R&D project registered as ANP nº 21475-9, “GeoBand – Geomodelagem de zona de dano em falhas geológicas” (PUC-Rio/CENPES/ANP),

sponsored by Petrobras. The authors also gratefully acknowledge the support from "Coordenação de Aperfeiçoamento de Pessoal de Nível Superior" (CAPES).

Authorship statement. The authors hereby confirm that they are the solely liable persons responsible for the authorship of this work and that all material that has been herein included as part of the present paper is either the property (and authorship) of the authors or has the permission of the owners to be included here.

References

[1] H. Fossen, *Structural Geology*. 2010. doi: 10.1088/1751-8113/44/8/085201.
[2] A. Torabi, T. S. S. Ellingsen, M. U. Johannessen, B. Alaei, A. Rotevatn, and D. Chiarella, "Fault zone architecture and its scaling laws: where does the damage zone start and stop?" *Geol. Soc. London, Spec. Publ.*, vol. 496, no. 1, pp. 99–124, 2020, doi: 10.1144/SP496-2018-151.
[3] S. Mayolle *et al.*, "Scaling of fault damage zones in carbonate rocks," *J. Struct. Geol.*, vol. 124, no. April, pp. 35–50, Jul. 2019, doi: 10.1016/j.jsg.2019.03.007.
[4] D. Qu and J. Tveranger, "Incorporation of deformation band fault damage zones in reservoir models," *Am. Assoc. Pet. Geol. Bull.*, vol. 100, no. 03, pp. 423–443, Mar. 2016, doi: 10.1306/12111514166.
[5] J.-H. Choi, P. Edwards, K. Ko, and Y.-S. Kim, "Definition and classification of fault damage zones: A review and a new methodological approach," *Earth-Science Rev.*, vol. 152, pp. 70–87, Jan. 2016, doi: 10.1016/j.earscirev.2015.11.006.
[6] J. Rohmer, T. K. Nguyen, and A. Torabi, "Off-fault shear failure potential enhanced by high-stiff/low-permeable damage zone during fluid injection in porous reservoirs," *Geophys. J. Int.*, vol. 202, no. 3, pp. 1566–1580, Sep. 2015, doi: 10.1093/gji/ggv225.
[7] Y.-S. Kim, D. C. P. Peacock, and D. J. Sanderson, "Fault damage zones," *J. Struct. Geol.*, vol. 26, no. 3, pp. 503–517, Mar. 2004, doi: 10.1016/j.jsg.2003.08.002.
[8] D. C. P. Peacock, V. Dimmen, A. Rotevatn, and D. J. Sanderson, "A broader classification of damage zones," *J. Struct. Geol.*, vol. 102, pp. 179–192, Sep. 2017, doi: 10.1016/j.jsg.2017.08.004.
[9] T. J. de Andrade, R. Quevedo, B. R. B. M. Carvalho, and D. Roehl, "Computational modeling of formation and evolution of damage zones in reservoir scale," in *Proceedings of the XLI Ibero-Latin-American Congress on Computational Methods in Engineering*, 2020, pp. 1–7.
[10] T. J. de Andrade, R. Quevedo, D. Roehl, R. De Janeiro, R. De Janeiro, and R. De Janeiro, "Numerical modeling of damage zones in rocks at reservoir scale using FEM," in *Proceedings of the XLII Ibero-Latin American Congress on Computational Methods in Engineering Ibero-Latin American Congress on Computational Methods in Engineering*, 2021, pp. 1–7.
[11] Y.-S. Kim and D. J. Sanderson, "The relationship between displacement and length of faults: a review," *Earth-Science Rev.*, vol. 68, no. 3–4, pp. 317–334, Jan. 2005, doi: 10.1016/j.earscirev.2004.06.003.
[12] A. Torabi and S. S. Berg, "Scaling of fault attributes: A review," *Mar. Pet. Geol.*, vol. 28, no. 8, pp. 1444–1460, Aug. 2011, doi: 10.1016/j.marpetgeo.2011.04.003.
[13] M. C. D. Kiewiet, "Comportamento hidromecanico de zonas de falha em travertino: Estudo Experimental e Numérico sobre o Impacto da Reativação Estrutural na Produção de Reservatórios," 2015.